A microscopic lattice model for liquid crystal elastomers

P. Pasini [a] G. Skačej [b,c],* C. Zannoni [b]

[a]*INFN, Sezione di Bologna, Via Irnerio 46, I-40126 Bologna, Italy*

[b]*Dipartimento di Chimica Fisica ed Inorganica and INSTM, Università di Bologna, Viale Risorgimento 4, I-40136 Bologna, Italy*

[c]*Oddelek za fiziko, Univerza v Ljubljani, Jadranska 19, SI-1000 Ljubljana, Slovenia*

Abstract

We propose a simple coarse-grained lattice model for liquid crystal elastomers and show, through large scale Monte Carlo simulations, that it can reproduce stress-strain, order, light transmission, and other experiments, including temperature effects. We focus both on homogeneously and inhomogeneously crosslinked materials.

Key words: liquid crystal elastomers, lattice models, Monte Carlo simulations
PACS: 61.30.Vx, 61.30.Cz, 61.41.+e

Liquid crystal elastomers (LCE) are fascinating materials, obtained by partially crosslinking chains of polymeric liquid crystals, that combine elastic properties of conventional rubbers with anisotropic properties of liquid crystals [1]. Because of the pronounced coupling between strain and alignment of mesogenic units, and the responsiveness to external stimuli such as temperature, electric and magnetic fields, or, in certain cases, UV light, LCE materials promise to be suitable for the construction of actuators and detectors, and for various applications, ranging from micro-pumps to artificial muscles [1,2]. On the fundamental side, irregular crosslinks and chemical heterogeneity in a LCE network provide a source of quenched random disorder similar to that observed in nematics with sprinkled silica nanoparticles [3–5], or in spin glasses with magnetic impurities [6] or random anisotropy [7]. Consequently, LCE, too, are characterized by a complex free energy landscape leading to glassy ordering. While, e.g., in spin glass systems quenched disorder can be overcome

* Corresponding author. Fax: +39.051.209.3690
  Email address: `gregor.skacej@fmf.uni-lj.si` (G. Skačej).

by a strong enough magnetic field, in LCE this can be achieved mechanically by stretching the sample [8]. Theoretically, LCE have been described, at continuum level, by the "neo-classical" theory based on anisotropic rubber elasticity [1], by Ginzburg-Landau approaches [9–11], as well as by 2D modeling [12]. It would, however, be very important to dispose of 3D microscopic models trying to catch the essential aspects of these complex systems and establish their microscopic roots. Here we develop a stretchable coarse-grained lattice model for LCE [13] by suitably generalizing similar models developed for liquid crystals [14,15]. The model is compared with experiment — polarized light transmission and deuterium nuclear magnetic resonance (^{2}H NMR) — carrying out constant-force Monte Carlo (MC) simulations of stretching experiments and temperature scans, both for homogeneously and inhomogeneously crosslinked (glassy) samples. Another lattice model has been presented recently [16] to explain the smoothness of the nematic-isotropic (NI) transition [11] in LCE. Also recently, stretching MC simulations of semiflexible polymer chain networks have been presented [17].
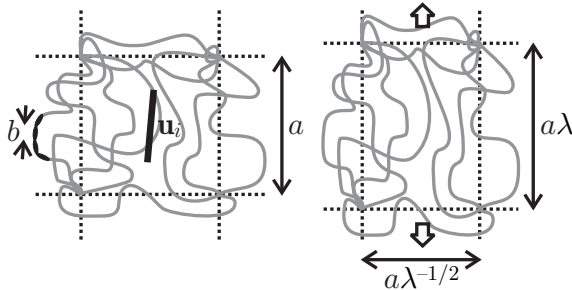

Fig. 1. Coarse-grained LCE model: undeformed (*left*) and stretched (*right*) unit cell (2D projection).

The main building blocks of our model are (i) rubber elasticity of polymer networks, (ii) anisotropic interactions between nematogenic units (van der Waals-type, or steric), and (iii) the strain-alignment coupling. (i) In the model, we assume the spatial distribution of crosslinks to be uniform (on average). The crosslinks are hence taken to coincide with lattice points of a 3D virtual "elastic" lattice (assumed simple cubic if undeformed, with spacing a), as sketched in Fig. 1. The neighboring crosslinks are connected by ideally flexible polymer chains that typically contain $\sim M$ monomers of length b each. We neglect chain entanglements and crosslink fluctuations, and work in the phantom chain limit [1]. Then, the distribution of chain end-to-end vectors is Gaussian and is isotropic as long as the sample is at rest but, upon stretching, polymer chain trajectories deform (assumed affinely and at constant volume) together with the sample. This decreases the chain conformation entropy thus giving a positive elastic free energy contribution. From the Gaussian end-to-end distribution, the probability of observing a unit cell deformed uniaxially by λ (the extension factor, see Fig. 1) is proportional to $\exp[-\alpha(\lambda^2 + 2/\lambda)]$, with $\alpha = 3a^2/2Mb^2$. In MC simulations, the same probability distribution in λ space is generated by the Metropolis algorithm [18] if a temperature-dependent

2

pseudo-Hamiltonian is introduced to mimic this entropic effect; see Ref. [19] and references therein. For uniform stretching (considered in the following) it is given by

$$\mathcal{H}_e = N k_B T \alpha \left(\lambda^2 + \frac{2}{\lambda} \right), \tag{1}$$

where N is the number of lattice sites. Assuming monomers to be almost close-packed ($a^3 \propto M b^3$), α scales as $M^{-1/3}$: short chains (and a higher crosslink density) yield a larger α and a higher elastic modulus. — (ii) A unit vector $\mathbf{u}_i$ representing the average orientation of mesogenic units (that needs not coincide with the polymer chain average direction) is placed in the center (Fig. 1) of each cell of the elastic lattice. Close-packed mesogenic clusters of the neighboring cells i and j (containing $\sim M$ units each) interact via

$$\mathcal{H}_u = - \sum_{\langle i < j \rangle} \epsilon_{ij} P_2(\mathbf{u}_i \cdot \mathbf{u}_j) \tag{2}$$

(assuming periodic boundary conditions), where $P_2(x) \equiv \frac{1}{2}(3x^2 - 1)$, and ϵ_{ij} are the nearest neighbor cell-cell interaction strengths. Their characteristic magnitude ϵ defines a reduced temperature scale $T^* = k_B T / |\epsilon|$ and we assume that the sign of ϵ_{ij} can vary according to polymer features. Thus, if the elastomer was crosslinked with mesogenic units aligned (i.e., in the nematic phase or under stress), we expect the system to relax to an aligned state. Choosing $\epsilon_{ij} = \epsilon > 0$ (< 0), $\mathcal{H}_u$ promotes parallel (perpendicular) alignment of $\mathbf{u}_i$ and is for $\epsilon > 0$ equivalent to the Lebwohl-Lasher (LL) lattice model used for nematics [14,15]. If, on the other hand, mesogenic units were not aligned prior to crosslinking, the relative equilibrium orientation of neighboring $\mathbf{u}_i$ and $\mathbf{u}_j$ is not necessarily parallel anymore. Irregularities that can emerge due to polymer chain disorder, enhanced by local chemical heterogeneities, can be mimicked by sampling ϵ_{ij} from a given distribution. The simultaneous presence of positive and negative ϵ_{ij} in the system (favoring parallel and perpendicular $\mathbf{u}_i$ alignment, respectively) creates a highly frustrated lattice system analogous, e.g., to a Heisenberg spin glass [6]. — (iii) Finally, the coupling between elastic strain and mesogenic alignment is modeled in terms of an effective mechanical field, again of entropic origin, directed along the major principal axis of strain. Then, if the sample is stretched by λ along the z-axis, the corresponding pseudo-Hamiltonian is assumed to be

$$\mathcal{H}_m = -k_B T \chi Q(\lambda) \sum_{i=1}^{N} P_2(\mathbf{u}_i \cdot \mathbf{z}), \tag{3}$$

where χ is a coupling constant and the deformation-dependent strength $Q(\lambda)$ is a second-rank order parameter associated with the net alignment of poly-

mer chains along $\mathbf{z}$. (Here $\mathbf{z}$ denotes a unit vector parallel to the z-axis.) Note that $\mathcal{H}_m$ is formally similar to the Maier-Saupe Hamiltonian in nematics, where the effective strength of the local aligning field on a given molecule is proportional to the order parameter of the surrounding nematic material [20,21]. Here, however, $Q(\lambda)$ measures the anisotropy of the polymer chain end-to-end tensor distribution, represented by a uniaxial ellipsoid $\mathcal{E}$ obtained from an isovolume deformation of a unit sphere by a factor of λ along the z-axis. Denoting with θ the polar angle measured with respect to $\mathbf{z}$, and with Ω the corresponding solid angle, the integration over $\mathcal{E}$ gives $Q(\lambda) = (4\pi)^{-1} \int_{\mathcal{E}} P_2(\cos\theta)d\Omega = (3\lambda^3/2)\mathcal{L}(\lambda^3 - 1) - 1/2$, where

$$\mathcal{L}(\zeta) = \begin{cases} \left(\operatorname{arctanh}\sqrt{-\zeta} - \sqrt{-\zeta}\right)/\sqrt{-\zeta^3}, & -1 < \zeta < 0, \\ 1/3, & \zeta = 0, \\ \left(\sqrt{\zeta} - \arctan\sqrt{\zeta}\right)/\sqrt{\zeta^3}, & \zeta > 0; \end{cases} \tag{4}$$

see Fig. 2, inset. In an undistorted sample ($\lambda = 1$) the mechanical field is absent and $Q(1) = 0$. On stretching ($\lambda > 1$) one has $Q(\lambda) > 0$, hence for $\chi > 0$ mesogenic units align along the stretch axis, while for $\chi < 0$ the alignment is perpendicular to it (vice versa when compressing). $Q(\lambda)$ is monotonically increasing for all $\lambda > 0$, with $Q(\lambda \to \infty) \to 1$. The sign and the magnitude of χ depend on the detailed molecular architecture of the elastomer. For instance, χ is found to be large and positive for strongly anisotropic main-chain elastomers [22]. For side-chain elastomers χ is positive and still substantial in magnitude when mesogens are attached to the polymer backbone side-on, while the end-on materials are characterized by a weaker coupling and a low χ value whose sign depends on the length of the connecting $-(CH_2)_n-$ spacer: odd and even n yield $\chi < 0$ and $\chi > 0$, respectively [1]. Note that in real elastomers the actual sign of χ can also depend on crosslinker type and concentration [23]. — $\mathcal{H}_m$, Eq. (3), also reproduces bulk director anchoring to the average chain direction (here $\mathbf{z}$), typical for LCE [1].

The total Hamiltonian of the model elastomer is given by $\mathcal{H} = \mathcal{H}_e + \mathcal{H}_u + \mathcal{H}_m$. We have tested if the model behavior resembles that of a real elastomer [1,8,9] performing constant-force MC simulations. In each MC cycle, first N reorientation moves $\mathbf{u}_i \to \mathbf{u}_i'$ were attempted, each accepted with probability $\min[1, \exp(-\Delta\mathcal{H}/k_B T)]$, where $\Delta\mathcal{H} = \mathcal{H}(\mathbf{u}_i', \lambda) - \mathcal{H}(\mathbf{u}_i, \lambda)$ [15,18,24]. These moves were followed by a constant-volume resize move $\lambda \to \lambda'$, accepted with probability $\min[1, \exp(-\Delta\mathcal{K}/k_B T)]$, where $\Delta\mathcal{K} = \mathcal{H}(\mathbf{u}_i, \lambda') - \mathcal{H}(\mathbf{u}_i, \lambda) + \epsilon N\sigma^*(\lambda - \lambda')$ [25], and $\sigma^* = \sigma a^3/\epsilon$ is the dimensionless engineering stress σ. (This procedure is similar to that used to control pressure, which is described in detail, e.g., in Ref. [26].) Trial move amplitudes were adjusted to maintain an acceptance ratio close to 50%. The sample size was set to $N = 30^3$ or 50^3. At least 6×10^4 equilibration and 6.6×10^4 production MC cycles

4

were performed. Stress and temperature scanning runs always used the last configuration of the preceding run to initialize the one to follow. In all simulations we have used: $\chi = 0.5$ (corresponding, e.g., to a main chain elastomer); $a = 4.6$ nm, $b = 1$ nm, and $M = 100$ (yielding $\alpha \approx 0.3$).

Fig. 2 (*top*) shows stress-strain isotherms $\lambda(\sigma^*)$ for a regularly crosslinked homogeneous sample with $\epsilon_{ij} = \epsilon > 0$ and 50^3 unit cells. At no stress ($\sigma^* = 0$) for $T^* \lesssim 1.141 \pm 0.003$ the system shows nematic order leading to a spontaneous elongation with $\lambda \approx 1.06$. Above this temperature the sample is isotropic and undeformed, $\lambda \approx 1$. For a ordinary LL model with $N = 50^3$ one has $T^*_{NI} \approx 1.123$ [27] and the shift of T^*_{NI} to higher T^* can be attributed to the presence of the aligning field, Eq. (3). When the sample is stretched in the nematic phase (curves a and b in Fig. 2), a Hookean (almost linear) $\lambda(\sigma^*)$ curve is observed. Taking $\epsilon \approx 0.023$ eV (from $T_{NI} \sim 300$ K), the Young modulus is $E \sim 52$ kPa, i.e., the material is rather soft, while $\sigma^* = 0.1$ corresponds to $\sigma \sim 3.8$ kPa. In this region the behavior is dominated by the elastic term $\mathcal{H}_e$, Eq. (1), so that $E \propto T$, which is a signature of entropic elasticity. On the other hand, when the sample is stretched from the isotropic phase, we find a stress-induced first-order aligning transition, observed experimentally [9], at a T^*-dependent value of σ^*. In this case the interplay of orientational ($\mathcal{H}_u$ and $\mathcal{H}_m$) and elastic ($\mathcal{H}_e$) terms is responsible for the massive alignment of mesogenic units. There is observable hysteresis on expansion and contraction, since
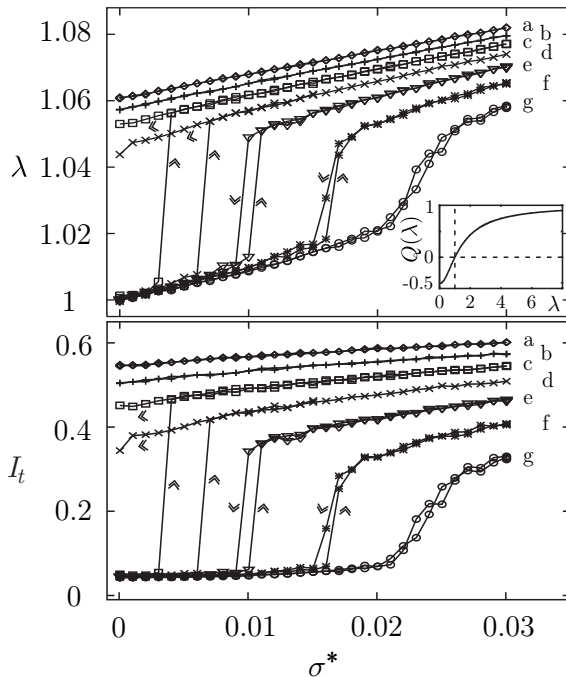

Fig. 2. Regular sample stretched: stress-strain isotherms (*top*) and light transmittance (*bottom*). Curves a-g correspond to $T^* = 1.135 - 1.15$, with a step size of 0.0025. Arrows denote the scan direction; note the hysteresis. Inset: $Q(\lambda)$ dependence.

for a 50^3 sample the order-disorder transition in the LL model is characterized by a free-energy barrier approaching $k_B T^*_{NI}$ [27]. At high enough temperature ($T^* \gtrsim 1.150$), however, the discontinuity in the aligning transition disappears and the $\lambda(\sigma^*)$ isotherms become continuous. In between the two regimes there is a critical point whose position is estimated as $\sigma^*_c = 0.021 \pm 0.002$, $T^*_c = 1.149 \pm 0.002$. Such critical stress-strain behavior has been predicted by de Gennes using symmetry arguments [28], and is similar also to the behavior of ordinary nematics exposed to, e.g., an electric field [29]. In our model, one can pass at fixed T^* from the continuous to the discontinuous regime also by reducing the α value (i.e., decreasing the crosslink density). Experimentally, equivalent observations are made when data for polymer melts (with no crosslinks) and for corresponding crosslinked networks are compared [30]. Conceivably, crosslinks could be gradually destroyed (or formed) by suitable treatments [31].

In a series of impressive experiments the optical behavior of LCE under stress has been studied [1,8,9]. As the sample is stretched in our simulation, the nematic director aligns along $\mathbf{z}$, the macroscopic order $P^z_2 = \langle P_2(\mathbf{u}_i \cdot \mathbf{z}) \rangle$ (averaged over lattice sites and MC cycles) increases and the sample becomes birefringent. We have used the simulated configurations to calculate the intensity transmitted when a linearly polarized beam, directed along the y-axis, impinges on a sample placed between crossed polarizers at $\pm 45°$ from $\mathbf{z}$. Light transmittance is given by $I_t = \sin^2(\pi d \Delta n / \lambda_0)$ [32], where d denotes sample thickness, λ_0 light wavelength, and Δn the refractive index anisotropy. For low Δn, $\Delta n \propto P^z_2$, and I_t depends on orientational ordering. In the simulation, light propagation within each pixel in the xz-plane is modeled using the Jones matrix formalism [32], assuming that local optical axes coincide with $\mathbf{u}_i$, and neglecting diffraction, as well as scattering [1]. To increase the optical thickness of the sample, $L = 10$ light passes were allowed for (yielding $d \approx 2.3~\mu$m) before averaging the transmitted light intensity over pixels to obtain I_t. Lateral contraction upon stretching ($d \propto \lambda^{-1/2}$) was taken into account as well. Other parameters: birefringence $\Delta n = 0.2175$ (for a perfectly ordered sample), and $\lambda_0 = 632.8$ nm (as for a He-Ne laser). The $I_t(\sigma^*)$ plot in Fig. 2 shows a strict correlation with the $\lambda(\sigma^*)$ curves. As long as the sample is isotropic, almost no light is transmitted, while a nonzero I_t is a signature of ordering in the system. Stretching irregular inhomogeneous samples generally yields a significantly smaller λ and P^z_2 at given σ^*, and the $\lambda(\sigma^*)$ curves become continuous. This is in agreement with the experimental observation that quenched disorder reduces the sharpness of the NI transition [11].

We now turn to an investigation of the effects of structural inhomogeneity and to temperature scan experiments. We have studied samples ($N = 30^3$) of four different LCE types, A-D, with increasing degree of quenched disorder obtained by allowing an inhomogeneity in the mesogen-mesogen interaction strength ϵ_{ij}. The first type, A, corresponds to a homogeneous LCE with $\epsilon_{ij} =$
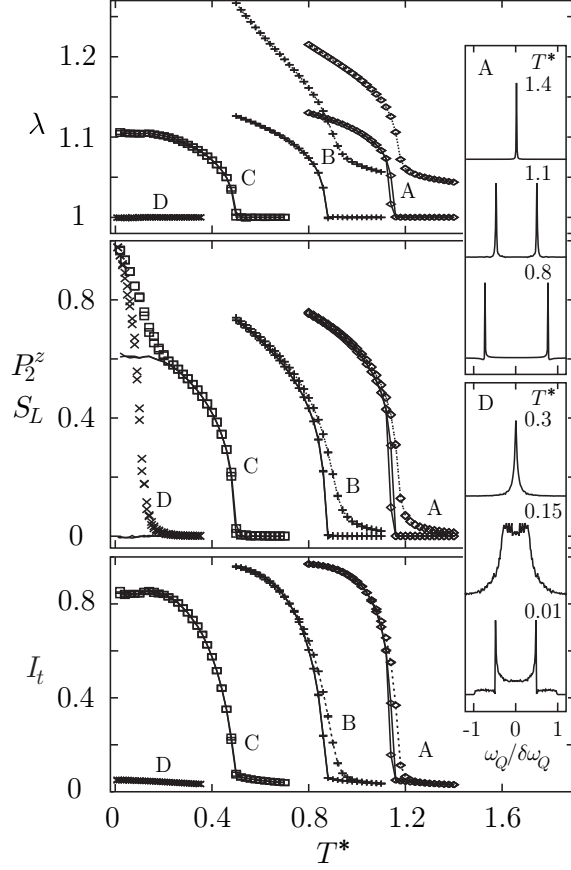
Fig. 3. Samples A-D: temperature scans. Sample length λ (*top*), P_2^z (lines) and S_L (symbols) order parameters (*center*), and transmittance I_t (*bottom*). No stress and $\sigma^* = 0.1$ (solid and dotted lines, respectively). Insets: ^{2}H NMR spectra for $\sigma^* = 0$; *top*: sample A, *bottom*: sample D.

ϵ, as before. For the B, C, and D types, ϵ_{ij} was sampled from a Gaussian distribution of width ϵ, centered at $\langle \epsilon_{ij} \rangle \approx 0.8\epsilon$, 0.5ϵ, and 0, respectively. Fig. 3 shows the average elongation and the degree of order for samples A-D, without stress and with $\sigma^* = 0.1$ (A-B only), against T^*. We see that when isotropic samples A-C are cooled down, at a well-defined temperature mesogenic units align to give nematic order. For unstressed sample A, the transition takes place at $T_A^* \approx 1.15 \pm 0.01$. The mechanical field-induced T_{NI}^* shift is slightly higher than in the larger 50^3 sample, possibly for a finite-size effect. Like in the LL model for nematics, the NI transition is weakly first-order, but hysteresis is less pronounced than in the 50^3 sample. If, however, the temperature scan is carried out under stress, for $\sigma^* = 0.1 > \sigma_c^*$ the supercritical regime is reached, and the transition is smeared out. In samples B and C, the NI transition shifts towards lower temperatures, with $T_B^* \approx 0.87 \pm 0.01$ and $T_C^* \approx 0.49 \pm 0.01$, suggesting that T_{NI}^* very roughly scales as $\langle \epsilon_{ij} \rangle$. The highly frustrated sample D, however, remains macroscopically disordered even as $T^* \to 0$, as suggested by $P_2^z \approx 0$ for all T^*. To check for local ordering at low T^*, we have introduced a "local" order parameter S_L, calculated as follows. For each unit cell the

MC cycle-averaged ordering matrix $\mathsf{Q}_i = \frac{1}{2}\langle 3\mathbf{u}_i \otimes \mathbf{u}_i - \mathsf{I}\rangle$ was calculated and diagonalized. Then the largest eigenvalue S_i and the local director $\mathbf{n}_i$ were identified, and finally $S_L = N^{-1}\sum_{i=1}^{N} S_i$. S_L takes the role of the Edwards-Anderson order parameter used for detecting local order in spin glasses [33]. The temperature dependence of S_L indeed shows local ordering in the system (for $T^* \lesssim 0.2$): orientational fluctuations of $\mathbf{u}_i$ are frozen-in along the local $\mathbf{n}_i$, which is analogous to glassy states observed in magnetic systems. The variance of S_L peaks at $T_g^* \approx 0.1$ and locates the transition to a locally ordered glassy state. Note that sample C (with $\langle\epsilon_{ij}\rangle \neq 0$) exhibits both the NI and the glass transition and thus qualitatively covers the elastomer behavior over a wide temperature range. Nematic alignment is accompanied by a spontaneous overall deformation of the sample: for $\chi > 0$ the sample is elongated on cooling. The deformation magnitude (here $\sim 10\%$) increases with increasing χ. In sample D for $\sigma^* = 0$ there is no macroscopic alignment and therefore no extension, while for $\sigma^* \neq 0$ and $T \to 0$ λ would become artificially large due to vanishing entropic elasticity [Eq. (1)] at very low temperatures; the corresponding curves are thus not reported. The transmittance $I_t(T^*)$, Fig. 3, is coherent with the behavior of P_2^z. Here $L = 15$ and $d \approx 2.07$ μm. Light scattering can again be neglected since refractive index inhomogeneities occur on length scales far below the wavelength of light, $a \ll \lambda_0$.

While light transmission methods measure the overall degree of orientational order, ^{2}H NMR can be used to probe local order in LCE [1,30,34] and hence distinguish between isotropic, aligned, and glassy states. Quadrupolar interactions in deuterated mesogenic units result in a frequency splitting $\omega_Q^j = \pm\delta\omega_Q P_2(\mathbf{u}_j\cdot\mathbf{b})$, where $\mathbf{b}$ is the orientation of the NMR spectrometer magnetic field $\mathbf{B}$ and $\delta\omega_Q$ is a coupling constant. To calculate NMR spectra, for $\mathbf{b}||\mathbf{z}$ we generated the free induction decay signal $G(t) = \langle\exp(i\int_0^t \omega_Q^j(t')\,dt')\rangle_j$, where $\langle...\rangle_j$ denotes ensemble averaging, and Fourier-transformed it [35]; neglecting diffusion. Typical line shapes for samples A and D are shown as insets in Fig. 3. Below T_{NI}^* homogeneous sample A gives double-peaked spectra, with peaks at $\omega_Q = \pm\delta\omega_Q P_2^z$. Glassy sample D below T_g^*, however, yields a Pake-type powder pattern, with a width proportional to S_L. Both results are consistent with order parameter data.

In conclusion, we have developed a simple and robust coarse-grained model for homogeneous and inhomogeneous liquid-crystalline elastomers undergoing uniaxial strain, with fixed director orientation. The stress-induced isotropic-nematic transition evolves from discontinuous to continuous with increasing temperature, as well as the elastic stiffness of the system. The model, however, is limited in describing soft elasticity as it cannot treat shear deformations. Temperature scans in samples with structural inhomogeneity, resulting in quenched disorder, reveal, apart from the standard NI transition, the onset of a macroscopically disordered glassy state with short-range order only, similar to that observed in magnetic systems. Our model seems thus capable

8

of describing various elastomer experiments, in particular stress-strain and temperature behavior. It contains only a small number of microscopic parameters: crosslink density, monomer size, number of monomers between neighboring crosslinks, the mesogen-mesogen interaction strength, and the strain-alignment coupling constant. We have linked these parameters to simulated experimental observables, transmitted light intensity and ^{2}H NMR spectra, giving therefore the model significant predictive power.

References

[1] M. Warner and E. M. Terentjev, Liquid Crystal Elastomers, Oxford University Press, Oxford, 2003.

[2] M. Hébert, R. Kant, and P.-G. de Gennes, J. de Physique I 7 (1997) 909.

[3] T. Bellini, M. Buscaglia, C. Chiccoli, F. Mantegazza, P. Pasini, and C. Zannoni, Phys. Rev. Lett. 85 (2000) 1008.

[4] T. Bellini, M. Buscaglia, C. Chiccoli, F. Mantegazza, P. Pasini, and C. Zannoni, Phys. Rev. Lett. 88 (2002) 245506.

[5] A. Arcioni, C. Bacchiocchi, I. Vecchi, G. Venditti, and C. Zannoni, Chem. Phys. Lett. 396 (2004) 433.

[6] D. Sherrington and S. Kirkpatrick, Phys. Rev. Lett. 35 (1975) 1792.

[7] R. Harris, M. Plischke, and M. J. Zuckermann, Phys. Rev. Lett. 31 (1973) 160.

[8] J. Küpfer and H. Finkelmann, Macromol. Chem. Rapid Commun. 12 (1991) 717.

[9] W. Kaufhold, H. Finkelmann, and H. R. Brand, Makromol. Chem. 192 (1991) 2555.

[10] N. Uchida and A. Onuki, Europhys. Lett. 45 (1999) 341.

[11] J. V. Selinger, H. G. Jeon, and B. R. Ratna, Phys. Rev. Lett. 89 (2002) 225701.

[12] Y.-K. Yu, P. L. Taylor, and E. M. Terentjev, Phys. Rev. Lett. 81 (1998) 128.

[13] G. Skačej, P. Pasini, and C. Zannoni, poster POLY-P019 presented at the 20th International Liquid Crystal Conference, Ljubljana, July 2004.

[14] P. A. Lebwohl and G. Lasher, Phys. Rev. A 6 (1972) 426.

[15] U. Fabbri and C. Zannoni, Mol. Phys. 58 (1986) 763.

[16] J. V. Selinger and B. R. Ratna, Phys. Rev. E 70 (2004) 041707.

[17] D. M. Bhawe, C. Cohen, and F. A. Escobedo, Phys. Rev. Lett. 93 (2004) 257804.

[18] N. Metropolis, A. W. Rosenbluth, M. N. Rosenbluth, A. H. Teller, and E. Teller, J. Chem. Phys. 21 (1953) 1087.

[19] G. Allegra and G. Raos, J. Chem. Phys. 116 (2002) 3109.

[20] W. Maier and A. Saupe, Z. Naturforsch. A 14 (1959) 882.

[21] W. Maier and A. Saupe, Z. Naturforsch. A 15 (1960) 287.

[22] B. Donnio, H. Wermter, and H. Finkelmann, Macromolecules 33 (2000) 7724.

[23] A. Greve and H. Finkelmann, Macromol. Chem. Phys. 202 (2001) 2926.

[24] P. Pasini and C. Zannoni, Advances in the Computer Simulations of Liquid Crystals, Kluwer, Dordrecht, 2000.

[25] G. Raos and G. Allegra, J. Chem. Phys. 113 (2000) 7554.

[26] D. Frenkel and B. Smit, Understanding Molecular Simulation, Academic Press, San Diego, 1996.

[27] N. V. Priezjev and R. A. Pelcovits, Phys. Rev. E 63, (2001) 062702.

[28] P.-G. de Gennes, C. R. Acad. Sc. Paris 281 (1975) 101.

[29] I. Lelidis and G. Durand, Phys. Rev. E 48 (1993) 3822.

[30] S. Disch, C. Schmidt, and H. Finkelmann, Macromol. Rapid Commun. 15 (1994) 303.

[31] F. La Mantia, Handbook of Plastics Recycling, Rapra Technology Limited, Shawbury, 2002.

[32] P. J. Collings and J. S. Patel, Handbook of Liquid Crystal Research, Oxford University Press, New York, 1997.

[33] S. F. Edwards and P. W. Anderson, J. Phys. F: Met. Phys. 5 (1975) 965.

[34] A. Lebar, Z. Kutnjak, S. Žumer, H. Finkelmann, A. Sánchez-Ferrer, and B. Zalar, Phys. Rev. Lett. 94 (2005) 197801.

[35] C. Chiccoli, P. Pasini, G. Skačej, S. Žumer, and C. Zannoni, Phys. Rev. E 60 (1999) 4219.